

Research Article

Sequence and structural variations determining the recruitment of WNK kinases to the KLHL3 E3 ligase

Zhuoyao Chen¹, Jinwei Zhang^{2,*}, Adrián R. Murillo-de-Ozores³, María Castañeda-Bueno³, Francesca D'Amico⁴, Raphael Heilig⁵, Charlotte E. Manning¹, Fiona J. Sorrell¹, Vincenzo D'Angiolella⁶, Roman Fischer⁵, Monique P. C. Mulder⁴, Gerardo Gamba^{3,7},  Dario R. Alessi² and  Alex N. Bullock¹

¹Centre for Medicines Discovery, New Biochemistry Building, University of Oxford, South Parks Road, Oxford OX1 3QU, U.K.; ²MRC Protein Phosphorylation and Ubiquitylation Unit, College of Life Sciences, University of Dundee, Dow Street, Dundee DD15EH, Scotland, U.K.; ³Department of Nephrology and Mineral Metabolism, Instituto Nacional de Ciencias Médicas y Nutrición Salvador Zubirán, Tlalpan, Mexico City, Mexico; ⁴Onco Institute and Department of Cell and Chemical Biology, Leiden University Medical Center (LUMC), Einthovenweg 20, 2333, ZC, Leiden, The Netherlands; ⁵Target Discovery Institute, Nuffield Department of Medicine, University of Oxford, Roosevelt Drive, Oxford OX3 7FZ, U.K.; ⁶Department of Oncology, Cancer Research U.K. and Medical Research Council Institute for Radiation Oncology, University of Oxford, Roosevelt Drive, Oxford OX3 7DQ, U.K.; ⁷Molecular Physiology Unit, Instituto de Investigaciones Biomédicas, Universidad Nacional Autónoma de México, Tlalpan, Mexico City, Mexico

Correspondence: Alex N. Bullock (alex.bullock@cmd.ox.ac.uk)



The BTB-Kelch protein KLHL3 is a Cullin3-dependent E3 ligase that mediates the ubiquitin-dependent degradation of kinases WNK1–4 to control blood pressure and cell volume. A crystal structure of KLHL3 has defined its binding to an acidic degron motif containing a PXXP sequence that is strictly conserved in WNK1, WNK2 and WNK4. Mutations in the second proline abrogate the interaction causing the hypertension syndrome pseudohypoaldosteronism type II. WNK3 shows a diverged degron motif containing four amino acid substitutions that remove the PXXP motif raising questions as to the mechanism of its binding. To understand this atypical interaction, we determined the crystal structure of the KLHL3 Kelch domain in complex with a WNK3 peptide. The electron density enabled the complete 11-mer WNK-family degron motif to be traced for the first time revealing several conserved features not captured in previous work, including additional salt bridge and hydrogen bond interactions. Overall, the WNK3 peptide adopted a conserved binding pose except for a subtle shift to accommodate bulkier amino acid substitutions at the binding interface. At the centre, the second proline was substituted by WNK3 Thr541, providing a unique phosphorylatable residue among the WNK-family degrons. Fluorescence polarisation and structural modelling experiments revealed that its phosphorylation would abrogate the KLHL3 interaction similarly to hypertension-causing mutations. Together, these data reveal how the KLHL3 Kelch domain can accommodate the binding of multiple WNK isoforms and highlight a potential regulatory mechanism for the recruitment of WNK3.

*Current address: Institute of Biomedical and Clinical Sciences, College of Medicine and Health, University of Exeter Medical School, Hatherly Laboratories, Streatham Campus, Exeter, EX4 4PS, U.K.

Received: 13 January 2022
Revised: 12 February 2022
Accepted: 18 February 2022

Accepted Manuscript online:
18 February 2022
Version of Record published:
4 March 2022

Introduction

WNK (with no lysine) kinases play a key role in mammalian blood pressure regulation [1–3]. WNKs, together with their downstream targets SPAK (SPS1-related proline/alanine-rich kinase) and OSR1 (oxidative stress-responsive kinase 1), regulate cation-chloride channels to achieve ion homeostasis in the kidney and neurons through a cascade of phosphorylation [3]. Four WNK isoforms (WNK1–4) are activated by autophosphorylation on a conserved serine in the kinase domain activation segment (WNK1 Ser382) upon exposure of cells to hypotonic and low [Cl[−]] conditions [4–6]. Activated WNK kinases then stimulate the kinase activity of SPAK/OSR1 by phosphorylating a conserved threonine residue in their kinase activation segments (SPAK Thr233, OSR1 Thr185) [7–9], which is facilitated by interaction between the SPAK/OSR1 CCT (Conserved C-terminal) domain and WNK RFXV/I peptide motifs [10,11]. Similarly, the SPAK/OSR1 CCT domain is recruited to RFXV/I motifs in the N-terminus of N[K]CC cation-chloride channels, and thereby phosphorylates conserved threonine

residues in their cytoplasmic domains to activate channel activity [10,12]. Conversely, phosphorylation on KCC cation-chloride channels by the WNK-SPAK/OSR1 axis has an inhibitory function [13]. Excessive activity of the WNK-SPAK/OSR1 cascade is the primary cause of PHAII (pseudohypoaldosteronism type II) hypertension and hyperkalemia syndrome [14].

Further regulation of WNK activity and blood pressure is provided by the Kelch-like protein 3 (KLHL3) E3 ligase, which ubiquitinates WNK1–4 to induce their degradation by the proteasome [15,16]. KLHL3 function is dependent on an N-terminal BTB domain and a C-terminal Kelch domain. The BTB domain was first identified as a conserved motif in the *Drosophila* proteins bric-à-brac, tramtrack and broad complex [17]. Similarly, the Kelch domain was originally described in the *Drosophila* protein Kelch (KEL) and comprises six kelch repeat motifs of 44–55 amino acids that fold into a six-bladed β -propeller structure [18,19]. As a BTB-Kelch family protein, KLHL3 forms the substrate adaptor of a cullin-RING ligase (CRL) complex consisting of cullin3, the RING domain protein RBX1 and KLHL3 [20]. Assembly into this complex is enabled by the N-terminal BTB domain which binds to cullin3, while the C-terminal Kelch domain serves to recruit the substrate proteins for ubiquitination [20,21]. The RBX1 subunit also binds to cullin3 and serves to recruit E2-ubiquitin conjugates to the CRL complex before the transfer of the ubiquitin onto WNK substrates. This substrate ubiquitination is promoted by the neddylation of cullin3, which induces a conformation favourable for conjugation of ubiquitin onto the WNK substrate [22–24].

Mutations in KLHL3 that disrupt interactions with either the WNK kinases or cullin3 lead to WNK up-regulation and the development of PHAII hypertension and hyperkalemia syndrome [15,16,25,26]. Similarly, mutations within the WNK4 acidic degron motif (residues 557–567) also cause PHAII hypertension syndrome [12,14] and occur within the recognition site for KLHL3 [27]. The structural basis for the interaction of KLHL3 and WNK4 has been recently determined and clearly defines the disruptive effects of PHAII-associated mutations in the complex interface [21].

The acidic degron motif in WNK4 is conserved among WNK1–4 allowing all four WNK family proteins to bind to KLHL3 [21]. However, WNK3 is notably distinguished by the presence of four amino acid substitutions in its acidic degron motif compared with the 11-mer WNK4 degron that was previously crystallized in complex with KLHL3 (Figure 1). These include substitutions at two proline sites in WNK4 that have potential to alter the peptide backbone. In addition, the WNK3 degron uniquely contains a threonine residue that potentially allows for a phosphorylation-dependant regulatory mechanism.

To address these differences, we report the 2.8 Å structure of the KLHL3 Kelch domain in complex with the WNK3 degron motif, as well as peptide binding assays that characterise the interactions of KLHL3 with variant WNK3 peptides. The new structure reveals a conserved structural mechanism for WNK family interaction with KLHL3 that explains the interactions of the four amino acid differences in WNK3. The structure and peptide binding assays also reveal that threonine phosphorylation in the WNK3 degron would disrupt the complex interface providing a potential regulatory mechanism for the KLHL3–WNK3 interaction.

Results

The WNK3 acidic degron motif binds potently to KLHL3 but does not bind if phosphorylated at Thr541

To investigate the binding of WNK3 variants to the KLHL3 Kelch domain we employed a fluorescence polarisation assay developed previously to map the degron motif of WNK4 (⁵⁵⁷EPEEADQHQ) [21]. In this assay, peptides containing the WNK family degron motif were conjugated to a Lumio green fluorophore and titrated with recombinant KLHL3 Kelch domain. Previous measurements indicated that the paralogs WNK1–4 could bind to KLHL3 with similarly high affinity (K_D values of 0.3–0.9 μ M) [21]. In agreement, we observed here that the 11-mer WNK3 degron motif (ECEETEVDQHV) bound to KLHL3 with $K_D = 0.67 \mu$ M (Figure 2). To examine whether modifications of the central Thr541 residue could form a potential regulatory mechanism we prepared an equivalent WNK3 peptide carrying a single phosphorylation at Thr541. Strikingly, the binding of this phospho-WNK3 peptide was too severely destabilised to measure a dissociation constant ($K_D > 50 \mu$ M, Figure 2). A similar loss of KLHL3 interaction was observed using a WNK3 T541E mutant degron (Figure 2). These observations were confirmed in a cellular model. WNK3 degradation upon co-transfection with KLHL3 was investigated in HEK293 cells. WNK3 levels in the presence of exogenous KLHL3 were significantly lower than in the absence of KLHL3, even at the lowest amounts of KLHL3 DNA used for transfection (Figure 3). In contrast, WNK3 T541E was noticeably resistant to degradation (Figure 3). Interestingly, T541A mutation also

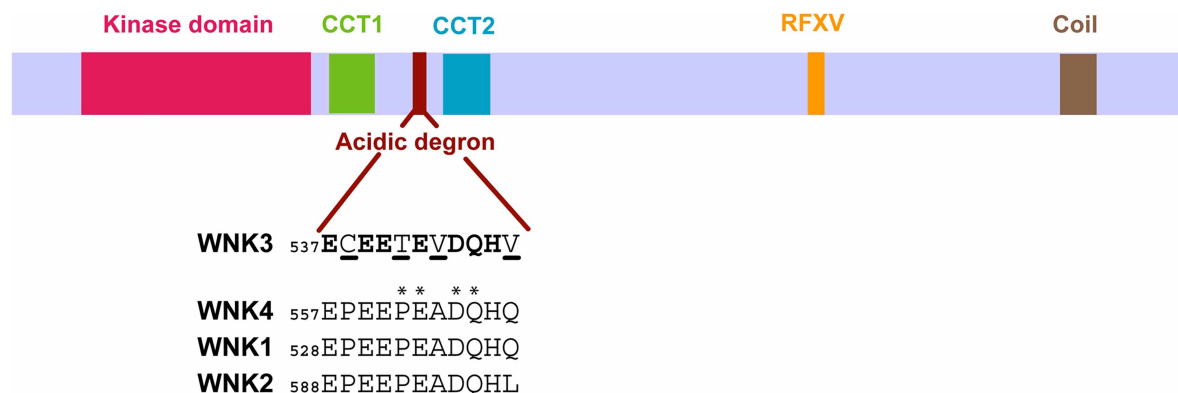


Figure 1. Schematic diagram showing the typical domain composition of WNK family kinases.

In addition to an N-terminal kinase domain, WNK1–4 contain an acidic degon motif that mediates their recruitment to the KLHL3 E3 ligase. Degron sequences are shown for each family member. The WNK3 degon motif contains four amino acid substitutions highlighted with underlined letters. Bold letters indicate conserved positions. Coil indicates a C-terminal coiled-coil domain. CCT-like is a circular permutant of the CCT domain of the OSR1 and SPAK kinases. WNK kinases contain additional RFXV or RFXI motifs (where X denotes any amino acid) that mediate their recruitment to the CCT domain of SPAK/OSR1. An asterisk denotes a site of mutation in WNK4 associated with PHAI hypertension syndrome (e.g. WNK4 P561L, E562K, D564A and Q565E) [14].

reduced KLHL3-mediated degradation of WNK3, showing that Thr at position 541 is important for WNK3 interaction with KLHL3. Together, these results indicated that WNK3 could bind to KLHL3 with similar potency to WNK4, and that WNK3 binding was abrogated upon modification of WNK3 Thr541.

Structure determination of the WNK3 acidic degon motif in complex with KLHL3

To investigate whether the divergent sequence of the WNK3 degon impacts upon its binding mode, we determined a 2.8 Å crystal structure of the 11-mer WNK3 degon in complex with the KLHL3 Kelch domain (Figure 4). Data processing and refinement statistics are presented in Table 1. The co-structure was solved in space group C2 2 2₁, with two WNK3 complexes in the asymmetric unit. The entire WNK3 peptide was traced in chain C (Figure 5A), but electron density was not resolved for the C-terminal residue Val547 in chain D

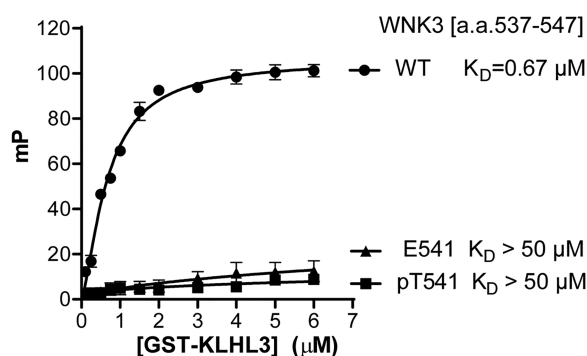


Figure 2. Analysis of the interaction between KLHL3 and WNK3 variants by fluorescence polarisation.

Purified GST-KLHL3 a.a. 298–587 was diluted appropriately and mixed at a 1 : 1 volume ratio with 20 nM Lumino-Green-labelled WNK3 peptides to the concentration stated in the Figure, with the peptide concentration consistent at 10 nM. Fluorescence polarisation measurements were recorded and corrected to the fluorescent probe alone. Each data point represents three technical replicates. One site-specific binding with hill slope was assumed and the disassociation constant was obtained. Binding curves, assuming one-site-specific binding, were then generated with Prism6 using milli-polarization (mP) units.

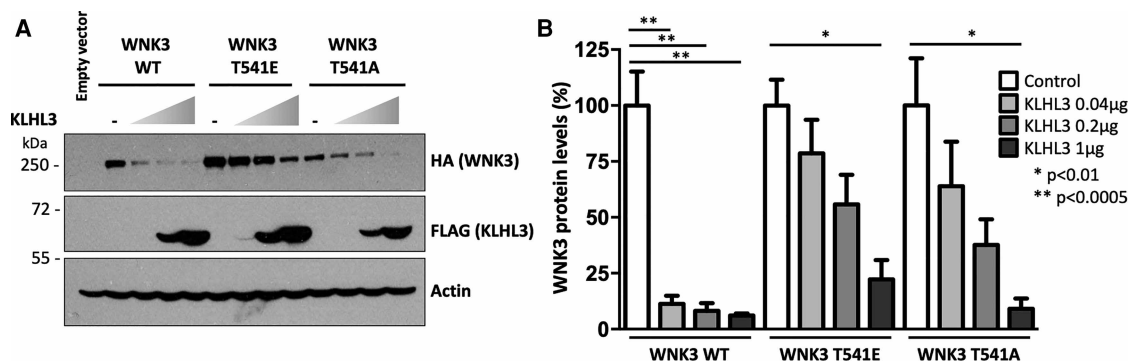


Figure 3. T541E substitution in WNK3 affects its KLHL3-targeted degradation in HEK293 cells.

(A) WNK3-HA protein levels were investigated in HEK293 cells transfected with either wild type or mutant constructs and increasing concentrations of KLHL3-FLAG. A representative blot is presented. (B) Quantitative results of three independent experiments. Data are mean \pm SEM. * $P < 0.01$, ** $P < 0.0005$.

(Figure 5B). In both WNK3 chains, Cys538 was observed to form a fortuitous, but likely artefactual, intermolecular disulfide-bond that potentially contributed to the observed crystal lattice. Despite distinct crystal contacts, the KLHL3 structure and WNK3 binding mode were highly conserved with the KLHL3–WNK4 complex (PDB 4CH9) suggesting a true representation of the physiologically relevant assembly.

Consistent with other family structures, the KLHL3 Kelch domain consists of six propeller blades arranged along a central axis. Each blade is folded as a twisted β -sheet comprising four antiparallel beta-strands. The WNK3 peptide sits atop the substrate-binding pocket, which is shaped by the six loops connecting the β B– β C strands, as well as the extended β D– β A loops that connect adjacent blades. Near identical conformations are observed for the peptide backbone in the two WNK3 chains, as well as side chains in the core interface, but several solvent-exposed side chains appear free to adopt alternative conformations, including Glu537, Cys538, Glu540 and His546 (Figure 5A,B).

Structural comparison of WNK3 and WNK4 binding to KLHL3

Of note for structural comparisons, the WNK3 and previous WNK4 co-structures were both determined under acidic conditions (pH 5.1 for WNK3 and pH 4.3 for WNK4), providing similar environments for electrostatic interactions. Overall, the bound peptides adopt a conserved conformation, containing an extended N-terminal segment that spans the two proline positions in WNK4, and a C-terminal segment that folds into a single

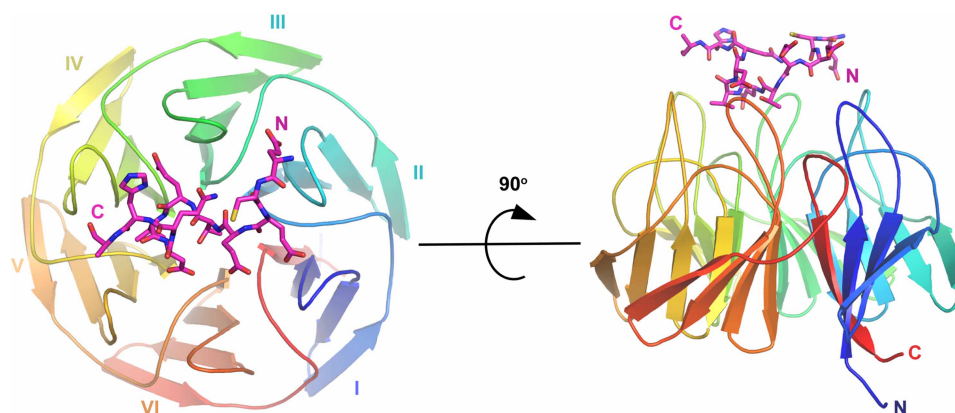


Figure 4. Crystal structure of the KLHL3 Kelch domain bound to WNK3 peptide determined at 2.8 Å.

Overview of the structure of the KLHL3 Kelch domain (rainbow ribbon) in complex with WNK3 peptide (purple sticks). Kelch repeats forming blades I to VI are labelled. N and C termini for both KLHL3 and WNK3 are labelled.

Table 1 Data collection and refinement statistics

Parameter	KLHL3–WNK3 peptide
Data collection	
Space group	C 2 2 21
Cell constants	
<i>a</i> , <i>b</i> , <i>c</i> (Å)	84.66, 169.72, 123.86
α , β , γ (°)	90, 90, 90
Resolution (Å)	50.02–2.8 (2.9–2.8)
Unique observations	22366 (2197)
Completeness (%)	99.98 (100.00)
<i>R</i> _{merge}	0.09155 (0.4966)
<i>I</i> / σ	8.18 (1.51)
Refinement	
Resolution (Å)	50.02–2.8
MR model	4CH9
Copies in ASU	2
<i>R</i> _{work} / <i>R</i> _{free}	0.2274/0.2496
Number of atoms	4566
Average B-factor (Å ²)	38.1
Average B-factor (protein) (Å ²)	38.1
Average B-factor (peptide) (Å ²)	43
Average B-factor (solvent) (Å ²)	37.5
RMSD (bonds) (Å)	0.007
RMSD (bonds) (°)	0.75

Values in parentheses indicate data for the highest resolution shell.

helical turn (Figures 4 and 5). The conserved glutamine in the WNK family degron motif acts to stabilise this turn through an intramolecular hydrogen bond, which in WNK3 is mediated between the side chain of Gln545 and the backbone carbonyl of Glu540 (Figure 5B,C). Mutation of this glutamine to glutamate in WNK4 is associated with hypertension and at physiological pH would remove the hydrogen bond donor for this intramolecular interaction.

Key differences in the two structures include the substitutions of WNK3 Cys538 and Thr541 at the two proline positions of WNK4. While the proline phi-psi angles are near ideal for extended structure (near -60° and $+135^\circ$, respectively), the substitutions in WNK3 are associated with a subtle shift (up to 1 Å) in the peptide backbone position. This shift appears favourable for the binding interface to accommodate the bulkier WNK3 Val543 substitution for WNK4 A563, as well as the branched Thr541 side chain for WNK4 Pro561.

A number of polar and hydrophobic interactions in the KLHL3–WNK3 structure are strongly conserved with the equivalent WNK4 complex. Perhaps the most important interaction is the salt bridge formed between WNK3 Asp544 and KLHL3 Arg528 (Figure 6). The substitution R528H in KLHL3 is the most frequent mutation in PHAII hypertension syndrome and is sufficient to abolish KLHL3 function [16,21]. Similarly, the aspartate position is associated with hypertension mutations in WNK4 (D564A) [14]. WNK3 Val543 is a conservative change from WNK4 Ala563 and packs adjacent to this salt bridge to form equivalent van der Waals interactions with KLHL3 Y449 and H498. The preceding WNK3 residue Glu542 is also buried at the KLHL3 surface between KLHL3 residues Tyr449 and Phe402, where it can hydrogen bond to KLHL3 Ser432. Finally, the backbone carbonyls of WNK3 Cys538 and Glu539 form conserved hydrogen bond interactions between KLHL3 side chains Arg360 and Arg339, respectively. Of note, the electron density maps suggest that Arg360 and Arg339 coordinate a buried chloride ion that is conserved in both the KLHL3–WNK3 and

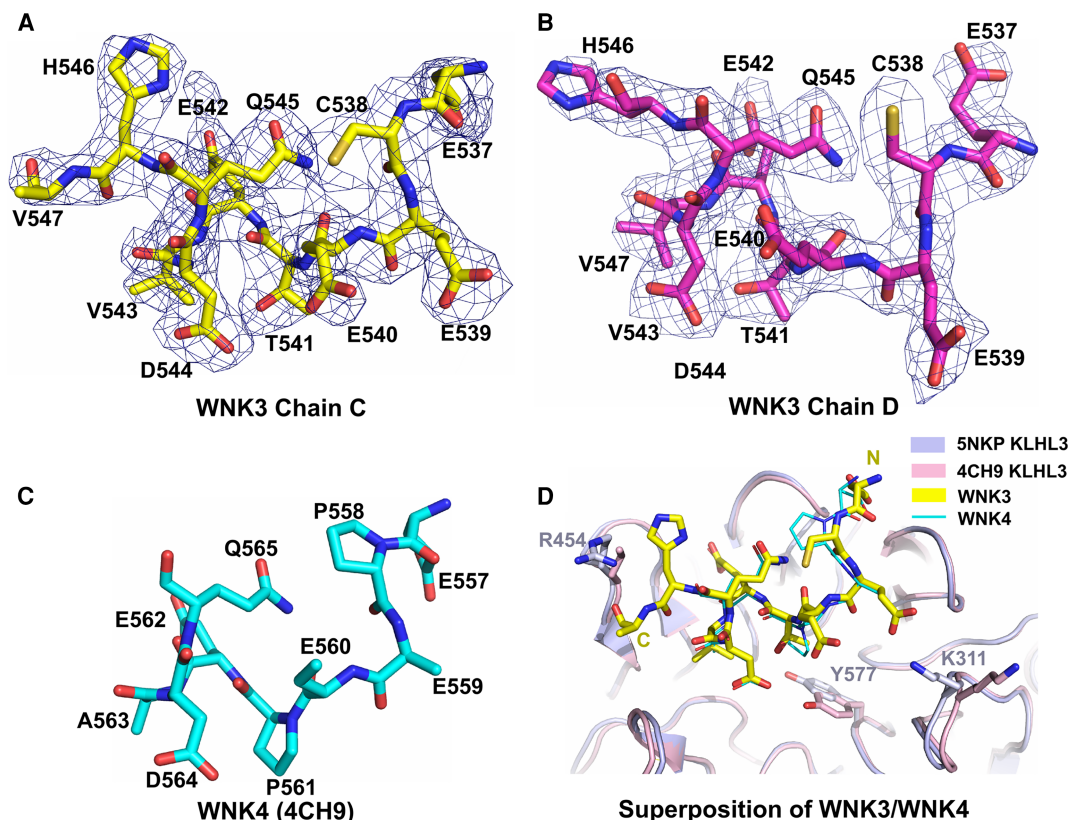


Figure 5. Structural comparison of WNK family degrons.

Stick representation and $2F_o - F_c$ electron density maps contoured at 1.0σ for (A) WNK3 chain C and (B) WNK3 chain D. WNK3 residues and their numbers are labelled (PDB 5NKP). (C) Stick representation of WNK4 degron peptide from PDB 4CH9. Residues are labelled as shown. (D) Superposition of the KLHL3–WNK3 and KLHL3–WNK4 complexes (PDBs 5NKP and 4CH9, respectively). The Kelch domains of KLHL3 are illustrated in ribbon representation. KLHL3 residues that adopt different conformations are highlighted with stick representation.

KLHL3–WNK4 complex structures (Supplementary Figure S1). Given the role of WNK kinases as chloride-sensors, we employed fluorescence polarisation measurements to investigate whether this interface chloride could modulate KLHL3 recruitment. However, no influence of chloride was observed (Supplementary Figure S2).

The WNK3 residues Glu542, Asp544 and Gln545 are strictly conserved in WNK4 (Figure 1), in which the equivalent Glu562, Asp564 and Gln565 are known sites of mutation in the PHAII hypertension syndrome [12,14]. Given the importance of these residues, it is perhaps unsurprising that their major interactions are also conserved. However, the side chain packing in the vicinity of the key salt bridge between WNK3 Asp544 and KLHL3 Arg528 is altered by the WNK3-specific substitutions of Thr541 and Val543 and a shift in the position of KLHL3 Tyr577 (Supplementary Figure S3).

Newly observed interactions in the WNK3 binding interface

The new KLHL3–WNK3 structure reveals several features of the WNK family degron interaction that were not previously defined. First, the full 11-mer degron motif can be traced in the WNK3 structure, whereas the two C-terminal residues were not observed in the WNK4 complex. Surprisingly, truncation of either of these residues was not tolerated in WNK4 showing their importance for the KLHL3 interaction [21]. The newly defined C-terminal residues, WNK3 His546 and Val547, appear flexible to pack on the surface of the Kelch domain forming van der Waals and electrostatic interactions with KLHL3 Tyr449 and Arg454, including a hydrogen bond between the backbone carbonyl of WNK3 Val547 (chain C) and KLHL3 Tyr449 (Figure 6). They also

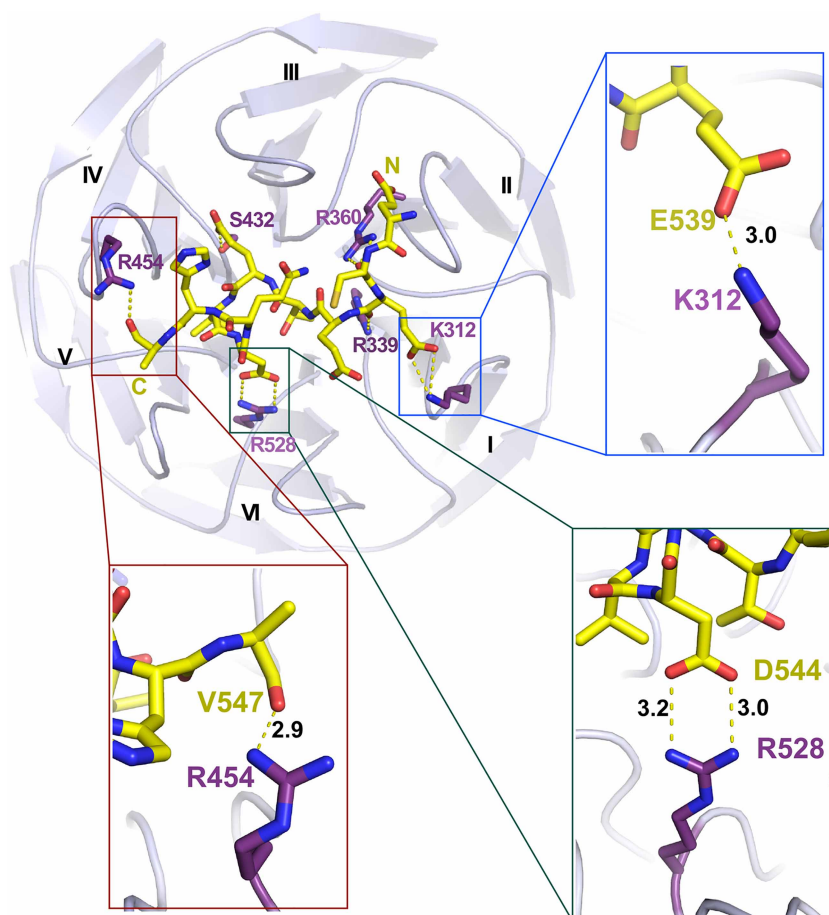


Figure 6. Hydrogen bond interactions in the KLHL3–WNK3 interface.

Overview of the polar contacts in the complex interface. KLHL3 residues are labelled in purple and WNK3 peptide is shown in yellow. Hydrogen bonds are demonstrated using dashed lines. Inset panels show selected contacts. Hydrogen bond distances (Å) are indicated.

contribute to the peptide's helical turn conformation through the backbone interactions of His546. Second, the new structure reveals a salt bridge between the conserved WNK3 residue Glu539 and KLHL3 Lys312 (Figure 6). The side chain atoms of this glutamate residue appeared disordered in the WNK4 structure, possibly resulting from its solvent exposed position and the additional flexibility of the associated lysine. These differences are also evident in a comparison of the buried interface surface areas for interacting residues in the two complex structures (Supplementary Figure S4).

Steric constraints would disfavour phosphothreonine in the WNK3 interface

WNK3 Thr541 adopts a central buried position in the complex interface and would appear to offer a unique potential phosphorylation site for regulation among the WNK family degron motifs (Figure 7A,B). The threonine side chain forms van der Waals interactions with several KLHL3 residues, including Arg339 and Tyr577 (Figure 7C,D). While too distant from KLHL3 Ser433 and Arg339 to form direct hydrogen bonds, there is also potential for these side chains to bind through water-mediated interactions that are not resolved at the 2.8 Å resolution of the structure.

To understand how post-translational modification on Thr541 might affect WNK3 binding to KLHL3, we modelled a phosphate moiety onto the threonine side chain using the ICM-Pro software package (Molsoft) [28]. When modelled in its crystallized conformation a severe steric clash was observed between pThr541 and WNK3 Asp544 that would break the critical salt bridge between this aspartate and KLHL3 R528 (Figure 7C).

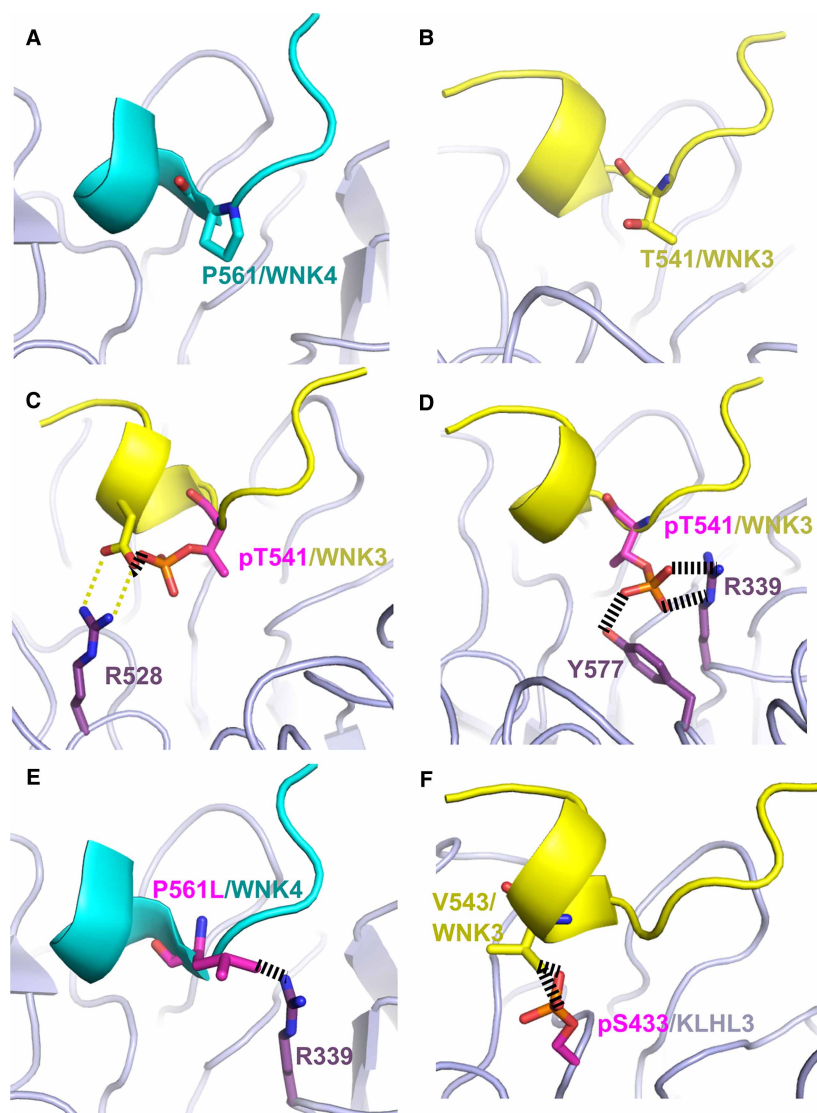


Figure 7. Steric constraints would disfavour phosphothreonine in the WNK3 interface.

(A) Location of WNK4 Pro561 at the centre of the KLHL3–WNK4 binding interface (PDB 4CH9). KLHL3 is shown in light purple and WNK4 is shown in light blue. (B) Similar position of WNK3 Thr541 in the structure of the KLHL3–WNK3 complex (PDB 5NKP). WNK3 is shown in yellow. (C) The modelling of a phosphothreonine in the crystallized conformation of WNK3 Thr541 reveals a severe steric clash with WNK3 Asp544 that would break the critical salt bridge (yellow dashed lines) between this aspartate and KLHL3 Arg528. (D) Alternative binding pose of WNK3 Thr541 suggested after an energy minimisation procedure to explore other potential side chain conformations. In this alternative pose, the phosphate moiety of pThr541 packs between KLHL3 Arg339 and Tyr577 in a sterically crowded environment that would bury the negative charge unfavourably without hydrogen bonding. (E) The modelling of a WNK4 PHAII mutation P561L reveals a steric clash (broken lines) with KLHL3 Arg339 that would disrupt the KLHL3–WNK4 interaction. (F) The modelling of Akt and PKA-dependent phosphorylation of KLHL3 Ser433 shows a severe steric clash with WNK3 Val543 that impairs KLHL3–WNK3 binding. The modelled residues in panels C–F are shown in pink.

We therefore performed an energy minimisation step to explore other potential side chain conformations. The resulting alternative conformation positioned the phosphate moiety of pThr541 between Arg339 and Tyr577 in a sterically crowded environment that would still bury the negative charge unfavourably without satisfying the required hydrogen bonding (Figure 7D). Thus, both the fluorescence polarisation assay and structural analysis

indicate that Thr541 phosphorylation would disrupt the WNK3–KLHL3 interaction and therefore serve as a potential regulatory mechanism.

The WNK3 degron motif resembles the preferred substrate sites of acidophilic kinases such as casein kinase II (CK2) [29]. However, to date there have been no reports of phosphorylation on WNK Thr541 either in the literature or in public databases. The majority of proteomic analyses use trypsin digestion to restrict cleavage sites to basic arginine and lysine positions, which simplifies database searches for peptide matches. We observed that WNK3 Thr541 lies in a particularly poor sequence region for this approach as trypsin digestion would yield a peptide 36 amino acids in length due to the paucity of surrounding basic residues. We reasoned therefore that a potential phosphorylation at this site may have been missed previously and decided to perform a new proteomic search using elastase cleavage which targets the more common positions of small hydrophobic residues [30]. For these experiments, we transfected HEK293T cells with Flag-tagged WNK3 plasmid and after 36 h treated the cells for 30 min with either isotonic or hypotonic buffer to allow for phosphorylation under different stimuli. Samples enriched for WNK3 were then prepared by anti-Flag immunoprecipitation, cleaved and analysed by mass spectrometry. Using this approach we obtained near complete coverage of the WNK3 sequence including the degron motif (Supplementary Figures S5, S6). Reassuringly, the experiment identified the known phosphorylation site within the kinase activation segment at Thr308. However, no phosphorylation was detected at the degron site residue Thr541 (Supplementary Figures S5, S6).

Overall, these results indicate that the four amino acid substitutions within the WNK3 acidic degron motif compared with WNK4 are well tolerated with no significant changes in the bound peptide conformation or binding affinity. We identify WNK3 Thr541 as a potential site for regulation, but further proteomic screening will be needed to demonstrate whether this site is phosphorylated under certain stimuli or in specific cell types.

Discussion

Relatively few of the ~600 human E3 ligases have been structurally characterised in complex with a bound substrate and only a small subset of these have had their structures solved with multiple partners to investigate potential differences in binding modes and regulation. To date, the only example within the BTB–Kelch family has been the redox sensor KEAP1 (KLHL19), which has been crystallised in complex with multiple partners, including the substrate Nrf2 [31–34] and the substrate competitors prothymosin alpha [35] and p62 (Sequestosome-1) [36,37]. These studies have defined notable substrate differences. For example, the divergent ‘ETGE’ and ‘DLG’ degron sites in Nrf2 have shown distinct binding affinities and bound peptide conformations [31]. Comparable KEAP1 structures have also been solved in complex with the related ‘STGE’ motif of p62 in both its serine phosphorylated [36] and non-phosphorylated forms [37]. In these structures, the phospho-serine provided p62 with enhanced binding affinity by mimicking the first glutamate of the Nrf2 ETGE motif [36].

Multiple substrates have been similarly identified for the KLHL3 E3 ligase, including the four members of the WNK kinase family, WNK1–4 [15,16,21]. WNK kinases display overlapping, but non-redundant functions reflecting with their different tissue expression profiles and regulation [3,12]. For example, loss of WNK3 may reduce ischemia-associated brain damage [38], whereas mutations in WNK1 and WNK4 disrupt renal salt uptake to induce pseudohypoaldosteronism type II (PHAII) [14]. Here, we investigated the variant degron motif of WNK3. Our fluorescence polarisation data confirmed that WNK3 binds to KLHL3 with comparable affinity to other WNK isoforms despite carrying four amino acid substitutions within its degron. These data also revealed that the binding was dependent on WNK3 Thr541. A mutation at the equivalent position in WNK4, P561L, causes PHAII showing the importance of this position for WNK kinase regulation [39] (Figure 7B).

The four substitutions in WNK3 remove a PXXP sequence motif that is conserved in the degrons of WNK1, WNK2 and WNK4 raising the question of whether the complex between WNK3 and KLHL3 may adopt a distinct binding mode. However, the new structure of the KLHL3–WNK3 complex reveals that the WNK3 peptide binds across the Kelch domain surface with a binding pose that is conserved with the equivalent WNK4 complex. In fact, the main difference appears to be a subtle shift at the binding interface to accommodate an alanine to valine substitution in WNK3, as well as WNK3 Thr541. The new structure also reveals several features of the degron interaction that were not previously defined. These include the salt bridge formed by the conserved WNK3 residue Glu539 and the additional packing interactions of the two C-terminal degron positions (WNK3 His546 and Val547) that contribute to the peptide’s helical turn conformation.

Outside of the WNK kinases, a PXXP degron sequence has also been recognised in proteins from the dishevelled (DVL1–3) family, which display a common PPGXPP degron motif for interaction with the Kelch domain

of KLHL12 [40,41]. Comparison of the peptide binding modes reveals a single common feature, but otherwise divergent structures (Supplementary Figure S7). In both instances, a single proline residue from each motif is used to anchor the degron at the centre of the Kelch domain pocket. In the example of the KLHL12–DVL1 complex, this interaction is mediated by the first proline in the PPGXPP motif (DVL1 Pro657), whereas the same interaction is mediated by the C-terminal proline in the WNK PXXP motif (WNK4 Pro561). The other regions of the proline-rich motifs are strikingly different in their binding modes and extend in opposite directions to contact different parts of the Kelch domains (Supplementary Figure S7). The DVL1 motif folds around the inside of the Kelch domain pocket to form contacts with multiple blades of the β -propeller, making particularly close contact with the large BC loops. In contrast, the WNK4 PXXP motif extends from the centre of the pocket solely towards blade 2 of the Kelch domain in KLHL3. These differences likely reflect the low sequence identity of 37% between the Kelch domains of KLHL3 and KLHL12.

Akt and PKA-dependent phosphorylation of KLHL3 Ser433 can impair the recruitment and ubiquitin-dependent degradation of WNK kinases [42,43]. Our structure reveals that this KLHL3 residue is positioned in close proximity to the bound WNK3 residues Val543 (3.85 Å) and Thr541 (4.9 Å), which would not tolerate the phospho-serine moiety due to a severe steric clash (Figure 7F). While no data are reported so far on phosphorylation of the WNK family degron, we hypothesised that a similar regulatory mechanism for degron binding may exist through the phosphorylation of WNK3 Thr541. Indeed, structural modelling and our fluorescence polarisation binding assay both indicated that this phosphorylation would disrupt the KLHL3–WNK3 interaction. Under hypotonic conditions, WNK3 mediates the inhibitory phosphorylation of KCC3 T991 and T1048 to restrict cell swelling in the brain [38,44]. We speculated whether such hypotonic conditions might promote the phosphorylation of WNK3 Thr541 to modulate WNK3 stability. Unfortunately, our proteomic studies were unable to detect evidence of pThr541 in HEK293T cells under either hypotonic or isotonic treatment. However, we cannot exclude that such phosphorylation occurs under other stimuli or in other specific cell types.

Overall, the current work extends our understanding of the molecular mechanisms that control WNK kinase ubiquitination and degradation. It shows that the four WNK family kinases share a conserved mechanism of binding to KLHL3 through an 11-mer acidic degron motif and highlights WNK3 Thr541 as a potential regulatory site for the E3 ligase interaction.

Materials and methods

Recombinant protein expression and purification

For fluorescence polarisation measurements of WNK3 variants, the Kelch domain of human KLHL3 (a.a. 290–587) was cloned into the bacterial expression vector pGEX6P-1 (MRC-PPU plasmid DU44387) and expressed as a GST fusion protein as previously described [21]. Briefly, *E. coli* BL21 cells were transformed with plasmid DNA and grown at 37°C in LB broth containing 100 µg/ml ampicillin until OD₆₀₀ reached 0.6. Cells were then cultured at 16°C for a further 16 h in the presence of 50 µM IPTG for protein induction. Harvested cells were lysed by sonication and the lysate clarified by centrifugation. GST fusion protein was affinity purified using 0.5 ml glutathione–sepharose beads and eluted in buffer (50 mM Tris–HCl pH 7.5, 150 mM NaCl, 2 mM DTT) containing 20 mM glutathione.

For structure determination and fluorescence polarisation investigation of chloride effects, human KLHL3 (a.a. 298–587) was cloned into the pNIC28-Bsa4 vector (Addgene plasmid #110251), which provides an N-terminal hexahistidine tag as previously described [21,45]. Expression was performed in BL21(DE3)-pRARE cells grown in LB broth containing 50 µg/ml kanamycin and 50 µg/ml chloramphenicol. When OD₆₀₀ reached 0.6, expression was induced overnight at 18°C by the addition of 0.4 mM IPTG. Cell pellets were lysed by sonication and recombinant protein purified using nickel-sepharose beads equilibrated in binding buffer (50 mM HEPES pH 7.5, 500 mM NaCl, 5% glycerol, 10 mM imidazole, 1 mM TCEP). Protein was eluted stepwise in buffers containing 100–500 mM imidazole. Further purification was achieved by size exclusion chromatography on a HiLoad 16/600 Superdex 200 pg column. The hexahistidine tag was cleaved using TEV protease and the correct mass of KLHL3 was confirmed by LC–MS mass spectrometry. Protein was stored in 50 mM HEPES pH 7.5, 300 mM NaCl, 0.5 mM TCEP, 2 mM DTT.

Fluorescence polarisation assay for the binding of WNK3 variants

Fluorescence polarisation measurements were performed at 25°C using KLHL3 Kelch domain (GST–KLHL3, a.a. 298–587, MRC-PPU plasmid DU44387) buffered in 50 mM Tris–HCl pH 7.5, 150 mM NaCl, 2 mM DTT.

All peptides (ECEETEVDQHV, WNK3 a.a. 537–547), (ECEET(P)EVDQHV, WNK3 a.a. 537–547, Thr541 is phosphorylated), and (EEEEEEVDQHV, WNK3 a.a. 537–547, Thr541 is mutated to Glu) were conjugated to the Lumio green fluorophore via an N-terminal linker (CCPGCCGGGG) and dialysed into assay buffer before use. Samples were prepared with 10 nM Lumio-green labelled peptide and the indicated concentration of protein in a final volume of 30 μ l. Fluorescence polarisation measurements were recorded using a BMG PheraStar plate reader, with an excitation wavelength of 485 nm and an emission wavelength of 538 nm, and measurements were corrected to the fluorescent probe alone. Data analysis and graphing were performed in GraphPad Prism6. One Site Specific binding with Hill Slope was assumed (model $Y = B_{\max} \times X^h / (K_D^h + X^h)$) and the disassociation constant, and associated standard error was obtained. All experimental bindings were repeated at least twice and comparable results to those shown in the present study were obtained.

Fluorescence polarisation assay for the effects of chloride concentration

Fluorescence polarisation measurements were performed at 25°C using KLHL3 Kelch domain (a.a. 298–587). The 11-residue degrons from WNK4 (EPEEPEADQHQ) and WNK3 (ECEETEVDQHV) were synthesised on a Syro II MultiSyntech Automated Peptide synthesiser using standard 9-fluorenylmethoxycarbonyl (Fmoc) based solid phase peptide chemistry on a Fmoc-a.a. preloaded Wang resin. After N-terminal labelling with Rhodamine-110 fluorophore, peptides were deprotected/cleaved from the resin and purified by HPLC. Samples were prepared with 10 nM Rhodamine-110 labelled peptide and the indicated indicated KLHL3 (a.a. 298–587) protein concentrations (from 0 to 3200 or 6400 nM) in a final volume of 20 μ l. Fluorescence polarisation measurements were recorded using a BMG PheraStar plate reader, with an excitation wavelength of 485 nm and an emission wavelength of 520 nm, and measurements were corrected to the fluorescent peptides alone (no protein). All individual bindings were performed in duplicates with 7 or 8 data points per curve. For K_D determination, data analysis and graphing were performed in GraphPad Prism; One Site total with NS (slope of non-specific binding) set to zero was assumed (model $Y = B_{\max} \times X / (K_D + X) + \text{Background}$).

Immunoblotting for WNK3 protein levels

HEK293 cells (ATCC® CRL-1573) were grown in Dulbecco's modified Eagle's medium (DMEM) supplemented with 10% fetal bovine serum to 70–80% confluence and transfected using Lipofectamine 2000 (Life Technologies, Inc.) with wild type or mutant WNK3-HA [46] and with different concentrations of KLHL3-FLAG [42]. Forty-eight hours post transfection, cells were lysed and protein concentration was quantified by the BCA protein assay (Pierce). Samples were diluted in Laemmli buffer and subjected to SDS-PAGE. Proteins were transferred to PVDF membranes which were then blocked for 1 h in 10% (w/v) non-fat milk dissolved in TBS- Tween 20 0.1% (TBSt). Antibodies were diluted in 5% (w/v) non-fat milk-TBSt. Incubation with HRP-coupled primary antibodies was performed overnight. Immunoblots were developed using radiographic film.

Lysis buffer: 50 mM Tris-HCl (pH 7.5), 1 mM EGTA, 1 mM EDTA, 50 mM sodium fluoride, 5 mM sodium pyrophosphate, 1 mM sodium orthovanadate, 1% (w/v) IGEPAL CA-630, 270 mM sucrose, 0.1% (v/v) 2-mercaptoethanol, and protease inhibitors (Complete tablets (Roche Applied Science)).

Crystallisation and structure determination

KLHL3 was concentrated to 9 mg/ml using a 10 kDa centrifugal concentrator (Millipore) and mixed with 2 mM WNK3 peptide (ECEETEVDQHV, synthesised by Severn Biotech Ltd). Crystallisation was performed using sitting drop vapour diffusion. Initial crystals obtained from coarse screens were used to make seed stocks for further fine screening. The best-diffracting crystals of the KLHL3–WNK3 complex were obtained at 4°C by mixing 20 nL seed stock with 75 nL of protein and 75 nL of a reservoir solution containing 6% PEG4K, 0.1 M acetate pH 5.1. Prior to vitrification in liquid nitrogen, crystals were cryoprotected by direct addition of reservoir solution supplemented with 25% ethylene glycol. Diffraction data were collected on beamline I03 at the Diamond Light Source, Didcot, U.K. Data were processed in PHENIX [47]. Molecular replacement was performed with Phaser MR in Phenix using PDB code 4CH9 chain A (Kelch domain of KLHL3) as the model. COOT [48] was used for manual model building and refinement, whereas PHENIX.REFINE [49] was used for automated refinement. TLS parameters were included at later stages of refinement. Structure factors and co-ordinates have been deposited in the PDB with accession code 5NKP.

Tissue culture and phosphorylation site mapping by LC–MS/MS

HEK293T cells were cultured in Dulbecco's modified Eagle's medium (DMEM, Gibco/Invitrogen) supplemented with 10% fetal bovine serum (FBS, Sigma–Aldrich), 100 U/ml penicillin sodium and 100 lg/ml streptomycin Sulfate (Sigma–Aldrich) in a humidified incubator at 37°C with 5% CO₂. For phospho-mapping experiments, full length human WNK3 (isoform 2) was cloned into a pCMV5-FLAG vector providing an N-terminal Flag affinity tag (MRC-PPU plasmid DU4949). Cells were split into 150 mm dishes and transfected with 14 µg Flag-WNK3 construct using polyethylenimine (Polysciences). Some 36 h post-transfection, culture medium was removed and the cells were treated with either isotonic buffer or hypotonic buffer to allow for phosphorylation under different stimuli. Isotonic high potassium buffer contained 20 mM HEPES pH 7.4, 95 mM NaCl, 50 mM KCl, 1 mM CaCl₂, 1 mM MgCl₂, 1 mM Na₂HPO₄, 1 mM Na₂SO₄. Hypotonic high potassium buffer contained 20 mM HEPES pH 7.4, 80 mM KCl, 1 mM CaCl₂, 1 mM MgCl₂, 1 mM Na₂HPO₄, 1 mM Na₂SO₄. Following 30 min incubation, cells were washed in PBS buffer and harvested for analysis. WNK3 was immunoprecipitated by anti-Flag M2 affinity resin (Sigma–Aldrich, A2220) and eluted with 3×Flag peptide. Protein samples were digested in elastase after DTT reduction, iodoacetamide alkylation and methanol-chloroform precipitation. The samples were then desalted using a SOLA HRP SPE Cartridge (Thermo Fisher, 60109-001) following the manufacturer's instruction.

Samples were analysed on a LC–MS/MS platform consisting of a Dionex Ultimate 3000 UPLC and Orbitrap Fusion Lumos mass spectrometer (both Thermo Fisher). Peptides were separated in a 60 min gradient from 2% ACN/5% DMSO in 0.1% Formic Acid to 35% ACN in the same buffer on a 50 cm Easy-Spray Column (Thermo Fisher). MS spectra were acquired in the Orbitrap with a resolution of 120 000 and with an ion target of 4×10^5 . MS/MS spectra were acquired in the ion trap in rapid mode after HCD fragmentation. Maximum injection time was set to 35 ms and AGC target was 4000. Selected precursors were excluded for 60 s.

LC–MS/MS data were analysed with PEAKS 7.0 against the Uniprot database using an Elastase digest pattern and 10 ppm/0.5 Da (MS/MS/MS) mass tolerance. Peptide level false discovery rate was adjusted to 1% and modifications were set according to the experimental parameters described above. LC–MS/MS data are available via ProteomeXchange with identifier PXD031606.

Data Availability

Structure factors and co-ordinates have been deposited in the PDB with accession code 5NKP. The mass spectrometry proteomics data have been deposited to the ProteomeXchange Consortium via the PRIDE [50] partner repository with the dataset identifier PXD031606 and 10.6019/PXD031606.

Competing Interests

The authors declare that there are no competing interests associated with the manuscript.

Funding

Z.C. acknowledges support from the China Scholarship Council — Nuffield Department of Medicine Scholarship. Z.C., A.N.B., C.E.M., F.J.S. acknowledge funding from the SGC, which is a registered charity (number 1097737) that receives funds from AbbVie, Bayer Pharma AG, Boehringer Ingelheim, Canada Foundation for Innovation, Eshelman Institute for Innovation, Genentech, Genome Canada through Ontario Genomics Institute [OGI-196], EU/EFPIA/OICR/McGill/KTH/Diamond Innovative Medicines Initiative 2 Joint Undertaking (EUbOPEN grant number 875510), Janssen, Merck & Co., MSD, Novartis Pharma AG, Pfizer, São Paulo Research Foundation-FAPESP, Takeda and Wellcome [grant 106169/ZZ14/Z]. F. D. acknowledges support from the European Union's Horizon 2020 research and innovation programme under the Marie Skłodowska-Curie grant agreement no. 813599. D.R.A. is supported by the Medical Research Council [grant number MC_UU_12016/2] and the pharmaceutical companies supporting the Division of Signal Transduction Therapy Unit (Boehringer-Ingelheim, GlaxoSmithKline, Merck KGaA -to D.R.A.). V.D.A. acknowledges support from the Medical Research Council (MRC grant MC_UU_00001/7) as well as Cancer Research UK (CR-UK grant no. C5255/A18085) through the Cancer Research UK Oxford Centre. Finally, we acknowledge grants from NIH No. DK51496 to G.G., grants from Conacyt Mexico No. 101720 to M.C.B. and A1-S-8290 to G.G., and a grant from PAPIIT UNAM No. IN201519 to G.G. J.Z. acknowledges funding from NIH Grants (No. R01 NS109358), Alzheimer's Research UK South West award (No. 112336), and The Royal Society UK (No. IEC\NSFC\201094).

Open Access Statement

Open access for this article was enabled by the participation of University of Oxford in an all-inclusive *Read & Publish* agreement with Portland Press and the Biochemical Society under a transformative agreement with JISC.

Author Contributions

A.N.B. and D.R.A. designed the research. J.Z. and F.D. performed the fluorescence polarisation assays. A.R.M.-O. and M.C.-B. performed the cellular binding and stability assays. Z.C. and C.E.M. purified KLHL3 protein. Z.C. crystallised the KLHL3–WNK3 complex and refined its structure with assistance from F.J.S. Z.C. performed tissue culture and sample preparation for phosphorylation mapping with assistance from V.D'A. LC–MS/MS was performed by R.H. and R.F. Research supervision was given by A.N.B., D.R.A., M.P.C.M., and G.G. The initial manuscript draft was prepared by A.N.B. and Z.C. and completed with the help of all authors.

CRedit Author Contribution

Alex N. Bullock: Conceptualization, Formal analysis, Supervision, Funding acquisition, Writing — original draft, Writing — review and editing. **Zhuoyao Chen:** Formal analysis, Validation, Investigation, Methodology, Writing — original draft, Writing — review and editing. **Jinwei Zhang:** Formal analysis, Investigation, Writing — review and editing. **Adrián Rafael Murillo-de-Ozores:** Formal analysis, Investigation, Writing — review and editing. **Maria Castañeda-Bueno:** Formal analysis, Investigation, Writing — review and editing. **Francesca D'Amico:** Formal analysis, Investigation, Writing — review and editing. **Raphael Heilig:** Formal analysis, Investigation, Writing — review and editing. **Charlotte E. Manning:** Resources, Writing — review and editing. **Fiona J. Sorrell:** Data curation, Supervision, Validation, Investigation, Writing — review and editing. **Vincenzo D'Angiolella:** Supervision, Writing — review and editing. **Roman Fischer:** Formal analysis, Supervision, Validation, Investigation, Project administration, Writing — review and editing. **Monique Mulder:** Data curation, Formal analysis, Supervision, Validation, Methodology, Writing — review and editing. **Gerardo Gamba:** Conceptualization, Formal analysis, Supervision, Validation, Methodology, Writing — review and editing. **Dario R. Alessi:** Supervision, Funding acquisition, Validation, Writing — review and editing.

Acknowledgements

The authors would like to thank Diamond Light Source for beamtime (proposal mx10619), as well as the staff of beamline I03 for assistance with crystal testing and data collection. Mass spectrometry analysis was performed at the Discovery Proteomics Facility (headed by Roman Fischer) which is part of the TDI MS Laboratory (led by Benedikt Kessler).

Abbreviations

BTB, Bric-a-brac, Tramtrack, and Broad complex; CCT, Conserved C-terminal; CRL3, Cullin3-dependent RING E3 ligase; DMEM, Dulbecco's modified Eagle's medium; DTT, Dithiothreitol; FBS, fetal bovine serum; GST, Glutathione S-transferase; HCD, Higher-energy collisional dissociation; HEK293T, human embryonic kidney 293 cell line expressing the SV40 large T antigen; IPTG, Isopropyl β -D-1-thiogalactopyranoside; KCC, K^+/Cl^- co-transporters; KLHL3, Kelch-like protein 3; LC/MS, Liquid chromatography-mass spectrometry; N[K]CC, Na^+/Cl^- ion co-transporters; NKCC2, $Na^+/K^+/2Cl^-$ co-transporter 2; OSR1, oxidative stress-responsive kinase 1; PDB, Protein Databank; PHAI1, pseudohypoaldosteronism type II; RING, really interesting new gene; SPAK, SPS1-related proline/alanine-rich kinase; TCEP, tris(2-carboxyethyl)phosphine; TEV, tobacco etch virus; WNK, with no lysine (K) kinase.

References

- 1 Murthy, M., Kurz, T. and O'Shaughnessy, K.M. (2017) WNK signalling pathways in blood pressure regulation. *Cell. Mol. Life Sci.* **74**, 1261–1280 <https://doi.org/10.1007/s00018-016-2402-z>
- 2 Murillo-de-Ozores, A.R., Chavez-Canales, M., de Los Heros, P., Gamba, G. and Castañeda-Bueno, M. (2020) Physiological processes modulated by the chloride-sensitive WNK-SPAK/OSR1 kinase signaling pathway and the cation-coupled chloride cotransporters. *Front. Physiol.* **11**, 585907 <https://doi.org/10.3389/fphys.2020.585907>
- 3 Alessi, D.R., Zhang, J., Khanna, A., Hochdorfer, T., Shang, Y. and Kahle, K.T. (2014) The WNK-SPAK/OSR1 pathway: master regulator of cation-chloride cotransporters. *Sci. Signal.* **7**, re3 <https://doi.org/10.1126/scisignal.2005365>

- 4 Thastrup, J.O., Rafiqi, F.H., Vitari, A.C., Pozo-Guisado, E., Deak, M., Mehellou, Y. et al. (2012) SPAK/OSR1 regulate NKCC1 and WNK activity: analysis of WNK isoform interactions and activation by T-loop trans-autophosphorylation. *Biochem. J.* **441**, 325–337 <https://doi.org/10.1042/BJ20111879>
- 5 Akella, R., Drozd, M.A., Humphreys, J.M., Jiou, J., Durbacz, M.Z., Mohammed, Z.J. et al. (2020) A phosphorylated intermediate in the activation of WNK kinases. *Biochemistry* **59**, 1747–1755 <https://doi.org/10.1021/acs.biochem.0c00146>
- 6 Xu, B.E., Min, X., Stippes, S., Lee, B.H., Goldsmith, E.J. and Cobb, M.H. (2002) Regulation of WNK1 by an autoinhibitory domain and autophosphorylation. *J. Biol. Chem.* **277**, 48456–48462 <https://doi.org/10.1074/jbc.M207917200>
- 7 Vitari, A.C., Deak, M., Morrice, N.A. and Alessi, D.R. (2005) The WNK1 and WNK4 protein kinases that are mutated in Gordon's hypertension syndrome phosphorylate and activate SPAK and OSR1 protein kinases. *Biochem. J.* **391**, 17–24 <https://doi.org/10.1042/BJ20051180>
- 8 Villa, F., Deak, M., Alessi, D.R. and van Aalten, D.M. (2008) Structure of the OSR1 kinase, a hypertension drug target. *Proteins* **73**, 1082–1087 <https://doi.org/10.1002/prot.22238>
- 9 Lee, S.J., Cobb, M.H. and Goldsmith, E.J. (2009) Crystal structure of domain-swapped STE20 OSR1 kinase domain. *Protein Sci.* **18**, 304–313 <https://doi.org/10.1002/pro.27>
- 10 Taylor, C.A. and Cobb, M.H. (2021) CCT and CCT-like modular protein interaction domains in WNK signaling. *Mol. Pharmacol.* **101**. <https://doi.org/10.1124/molpharm.121.000307>
- 11 Villa, F., Goebel, J., Rafiqi, F.H., Deak, M., Thastrup, J., Alessi, D.R. et al. (2007) Structural insights into the recognition of substrates and activators by the OSR1 kinase. *EMBO Rep.* **8**, 839–845 <https://doi.org/10.1038/sj.embor.7401048>
- 12 Richardson, C. and Alessi, D.R. (2008) The regulation of salt transport and blood pressure by the WNK-SPAK/OSR1 signalling pathway. *J. Cell Sci.* **121**, 3293–3304 <https://doi.org/10.1242/jcs.029223>
- 13 de Los Heros, P., Alessi, D.R., Gourlay, R., Campbell, D.G., Deak, M., Macartney, T.J. et al. (2014) The WNK-regulated SPAK/OSR1 kinases directly phosphorylate and inhibit the K⁺-Cl[−] co-transporters. *Biochem. J.* **458**, 559–573 <https://doi.org/10.1042/BJ20131478>
- 14 Wilson, F.H., Disse-Nicodeme, S., Choate, K.A., Ishikawa, K., Nelson-Williams, C., Desitter, I. et al. (2001) Human hypertension caused by mutations in WNK kinases. *Science* **293**, 1107–1112 <https://doi.org/10.1126/science.1062844>
- 15 Wakabayashi, M., Mori, T., Isobe, K., Sahara, E., Susa, K., Araki, Y. et al. (2013) Impaired KLHL3-mediated ubiquitination of WNK4 causes human hypertension. *Cell Rep.* **3**, 858–868 <https://doi.org/10.1016/j.celrep.2013.02.024>
- 16 Ohta, A., Schumacher, F.R., Mehellou, Y., Johnson, C., Knebel, A., Macartney, T.J. et al. (2013) The CUL3-KLHL3 E3 ligase complex mutated in Gordon's hypertension syndrome interacts with and ubiquitylates WNK isoforms: disease-causing mutations in KLHL3 and WNK4 disrupt interaction. *Biochem. J.* **451**, 111–122 <https://doi.org/10.1042/BJ20121903>
- 17 Stogios, P.J., Downs, G.S., Jauhal, J.J., Nandra, S.K. and Prive, G.G. (2005) Sequence and structural analysis of BTB domain proteins. *Genome Biol.* **6**, R82 <https://doi.org/10.1186/gb-2005-6-10-r82>
- 18 Hudson, A.M. and Cooley, L. (2010) Drosophila Kelch functions with Cullin-3 to organize the ring canal actin cytoskeleton. *J. Cell Biol.* **188**, 29–37 <https://doi.org/10.1083/jcb.200909017>
- 19 Bork, P. and Doolittle, R.F. (1994) Drosophila kelch motif is derived from a common enzyme fold. *J. Mol. Biol.* **236**, 1277–1282 [https://doi.org/10.1016/0022-2836\(94\)90056-6](https://doi.org/10.1016/0022-2836(94)90056-6)
- 20 Ji, A.X. and Prive, G.G. (2013) Crystal structure of KLHL3 in complex with Cullin3. *PLoS ONE* **8**, e60445 <https://doi.org/10.1371/journal.pone.0060445>
- 21 Schumacher, F.R., Sorrell, F.J., Alessi, D.R., Bullock, A.N. and Kurz, T. (2014) Structural and biochemical characterization of the KLHL3-WNK kinase interaction important in blood pressure regulation. *Biochem. J.* **460**, 237–246 <https://doi.org/10.1042/BJ20140153>
- 22 Duda, D.M., Borg, L.A., Scott, D.C., Hunt, H.W., Hammel, M. and Schulman, B.A. (2008) Structural insights into NEDD8 activation of cullin-RING ligases: conformational control of conjugation. *Cell* **134**, 995–1006 <https://doi.org/10.1016/j.cell.2008.07.022>
- 23 Baek, K., Krist, D.T., Prabu, J.R., Hill, S., Klugel, M., Neumaier, L.M. et al. (2020) NEDD8 nucleates a multivalent cullin-RING-UBE2D ubiquitin ligation assembly. *Nature* **578**, 461–466 <https://doi.org/10.1038/s41586-020-2000-y>
- 24 Baek, K., Scott, D.C. and Schulman, B.A. (2021) NEDD8 and ubiquitin ligation by cullin-RING E3 ligases. *Curr. Opin. Struct. Biol.* **67**, 101–109 <https://doi.org/10.1016/j.sbi.2020.10.007>
- 25 Boyden, L.M., Choi, M., Choate, K.A., Nelson-Williams, C.J., Farhi, A., Toka, H.R. et al. (2012) Mutations in kelch-like 3 and cullin 3 cause hypertension and electrolyte abnormalities. *Nature* **482**, 98–102 <https://doi.org/10.1038/nature10814>
- 26 Louis-Dit-Picard, H., Barc, J., Trujillano, D., Miserey-Lenkei, S., Bouatia-Naji, N., Pylypenko, O. et al. (2012) KLHL3 mutations cause familial hyperkalemic hypertension by impairing ion transport in the distal nephron. *Nat. Genet.* **44**, 456–460. S451–S453 <https://doi.org/10.1038/ng.2218>
- 27 Shibata, S., Zhang, J., Puthumana, J., Stone, K.L. and Lifton, R.P. (2013) Kelch-like 3 and Cullin 3 regulate electrolyte homeostasis via ubiquitination and degradation of WNK4. *Proc. Natl Acad. Sci. U.S.A.* **110**, 7838–7843 <https://doi.org/10.1073/pnas.1304592110>
- 28 Abagyan, R., Totrov, M. and Kuznetsov, D. (1994) Icm — a new method for protein modeling and design: applications to docking and structure prediction from the distorted native conformation. *J. Comput. Chem.* **15**, 488–506 <https://doi.org/10.1002/jcc.540150503>
- 29 Miller, M.L., Jensen, L.J., Diella, F., Jorgensen, C., Tinti, M., Li, L. et al. (2008) Linear motif atlas for phosphorylation-dependent signaling. *Sci. Signal.* **1**, ra2 <https://doi.org/10.1126/scisignal.1159433>
- 30 Davis, S., Charles, P.D., He, L., Mowlds, P., Kessler, B.M. and Fischer, R. (2017) Expanding proteome coverage with CHarge ordered parallel ion aNalysis (CHOPIN) combined with broad specificity proteolysis. *J. Proteome Res.* **16**, 1288–1299 <https://doi.org/10.1021/acs.jproteome.6b00915>
- 31 Tong, K.I., Padmanabhan, B., Kobayashi, A., Shang, C., Hirotsu, Y., Yokoyama, S. et al. (2007) Different electrostatic potentials define ETGE and DLG motifs as hinge and latch in oxidative stress response. *Mol. Cell. Biol.* **27**, 7511–7521 <https://doi.org/10.1128/MCB.00753-07>
- 32 Fukutomi, T., Takagi, K., Mizushima, T., Ohuchi, N. and Yamamoto, M. (2014) Kinetic, thermodynamic, and structural characterizations of the association between Nrf2-DLGex degron and Keap1. *Mol. Cell. Biol.* **34**, 832–846 <https://doi.org/10.1128/MCB.01191-13>
- 33 Padmanabhan, B., Tong, K.I., Ohta, T., Nakamura, Y., Scharlock, M., Ohtsui, M. et al. (2006) Structural basis for defects of Keap1 activity provoked by its point mutations in lung cancer. *Mol. Cell* **21**, 689–700 <https://doi.org/10.1016/j.molcel.2006.01.013>
- 34 Lo, S.C., Li, X., Henzl, M.T., Beamer, L.J. and Hannink, M. (2006) Structure of the Keap1:Nrf2 interface provides mechanistic insight into Nrf2 signaling. *EMBO J.* **25**, 3605–3617 <https://doi.org/10.1038/sj.emboj.7601243>
- 35 Padmanabhan, B., Nakamura, Y. and Yokoyama, S. (2008) Structural analysis of the complex of Keap1 with a prothymosin alpha peptide. *Acta Crystallogr. Sect. F Struct. Biol. Cryst. Commun.* **64**, 233–238 <https://doi.org/10.1107/S1744309108004995>

- 36 Ichimura, Y., Waguri, S., Sou, Y.S., Kageyama, S., Hasegawa, J., Ishimura, R. et al. (2013) Phosphorylation of p62 activates the Keap1-Nrf2 pathway during selective autophagy. *Mol. Cell* **51**, 618–631 <https://doi.org/10.1016/j.molcel.2013.08.003>
- 37 Komatsu, M., Kurokawa, H., Waguri, S., Taguchi, K., Kobayashi, A., Ichimura, Y. et al. (2010) The selective autophagy substrate p62 activates the stress responsive transcription factor Nrf2 through inactivation of Keap1. *Nat. Cell Biol.* **12**, 213–223 <https://doi.org/10.1038/ncb2021>
- 38 Begum, G., Yuan, H., Kahle, K.T., Li, L., Wang, S., Shi, Y. et al. (2015) Inhibition of WNK3 kinase signaling reduces brain damage and accelerates neurological recovery after stroke. *Stroke* **46**, 1956–1965 <https://doi.org/10.1161/STROKEAHA.115.008939>
- 39 Gong, H., Tang, Z., Yang, Y., Sun, L., Zhang, W., Wang, W. et al. (2008) A patient with pseudohypoadosteronism type II caused by a novel mutation in WNK4 gene. *Endocrine* **33**, 230–234 <https://doi.org/10.1007/s12020-008-9084-8>
- 40 Chen, Z., Wasney, G.A., Picaud, S., Filippakopoulos, P., Vedadi, M., D'Angiolella, V. et al. (2020) Identification of a PGXP deproton motif in dishevelled and structural basis for its binding to the E3 ligase KLHL12. *Open Biol.* **10**, 200041 <https://doi.org/10.1098/rsob.200041>
- 41 Zhao, B., Payne, W.G., Sai, J., Lu, Z., Olejniczak, E.T. and Fesik, S.W. (2020) Structural elucidation of peptide binding to KLHL-12, a substrate specific adapter protein in a Cul3-ring E3 ligase complex. *Biochemistry* **59**, 964–969 <https://doi.org/10.1021/acs.biochem.9b01073>
- 42 Shibata, S., Arroyo, J.P., Castaneda-Bueno, M., Puthumana, J., Zhang, J., Uchida, S. et al. (2014) Angiotensin II signaling via protein kinase C phosphorylates Kelch-like 3, preventing WNK4 degradation. *Proc. Natl Acad. Sci. U.S.A.* **111**, 15556–15561 <https://doi.org/10.1073/pnas.1418342111>
- 43 Yoshizaki, Y., Mori, Y., Tsuzaki, Y., Mori, T., Nomura, N., Wakabayashi, M. et al. (2015) Impaired degradation of WNK by Akt and PKA phosphorylation of KLHL3. *Biochem. Biophys. Res. Commun.* **467**, 229–234 <https://doi.org/10.1016/j.bbrc.2015.09.184>
- 44 Zhao, H., Nepomuceno, R., Gao, X., Foley, L.M., Wang, S., Begum, G. et al. (2017) Deletion of the WNK3-SPAK kinase complex in mice improves radiographic and clinical outcomes in malignant cerebral edema after ischemic stroke. *J. Cereb. Blood Flow Metab.* **37**, 550–563 <https://doi.org/10.1177/0271678X16631561>
- 45 Strain-Damerell, C., Mahajan, P., Fernandez-Cid, A., Gileadi, O. and Burgess-Brown, N.A. (2021) Screening and production of recombinant human proteins: ligation-independent cloning. *Methods Mol. Biol.* **2199**, 23–43 https://doi.org/10.1007/978-1-0716-0892-0_3
- 46 Castaneda-Bueno, M., Arroyo, J.P., Zhang, J., Puthumana, J., Yarborough, Ill, O., Shibata, S. et al. (2017) Phosphorylation by PKC and PKA regulate the kinase activity and downstream signaling of WNK4. *Proc. Natl Acad. Sci. U.S.A.* **114**, E879–E886 <https://doi.org/10.1073/pnas.1620315114>
- 47 Adams, P.D., Afonine, P.V., Bunkoczi, G., Chen, V.B., Davis, I.W., Echols, N. et al. (2010) PHENIX: a comprehensive Python-based system for macromolecular structure solution. *Acta Crystallogr. D Biol. Crystallogr.* **66**, 213–221 <https://doi.org/10.1107/S0907444909052925>
- 48 Emsley, P., Lohkamp, B., Scott, W.G. and Cowtan, K. (2010) Features and development of Coot. *Acta Crystallogr. D Biol. Crystallogr.* **66**, 486–501 <https://doi.org/10.1107/S0907444910007493>
- 49 Afonine, P.V., Grosse-Kunstleve, R.W., Echols, N., Headd, J.J., Moriarty, N.W., Mustyakimov, M. et al. (2012) Towards automated crystallographic structure refinement with phenix.refine. *Acta Crystallogr. D Biol. Crystallogr.* **68**, 352–367 <https://doi.org/10.1107/S0907444912001308>
- 50 Perez-Riverol, Y., Csordas, A., Bai, J., Bernal-Llinares, M., Hewapathirana, S., Kundu, D.J. et al. (2019) The PRIDE database and related tools and resources in 2019: improving support for quantification data. *Nucleic Acids Res.* **47**, D442–D450 <https://doi.org/10.1093/nar/gky1106>

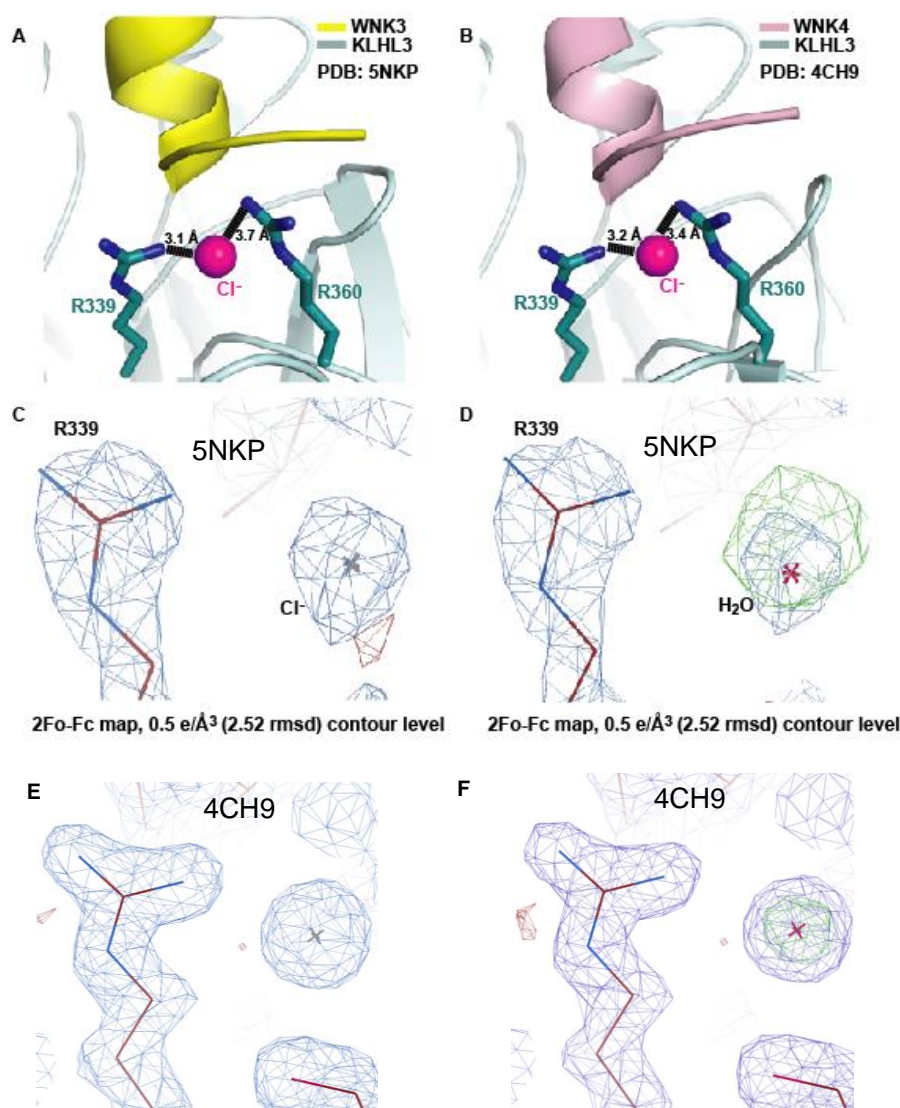


Figure S1. Bound chloride ions in the KLHL3-WNK3 and KLHL3-WNK4 structures. (A and B) A bound chloride ion is observed in the KLHL3-WNK3 and KLHL3-WNK4 complexes and forms electrostatic interactions with positive charged Arg339 and Arg360 in KLHL3. KLHL3 residues are labelled in green, WNK3 peptide is shown in yellow, and WNK4 peptide is shown in pale pink. The chloride ions are shown as magenta spheres. The electrostatic interactions are demonstrated using dashed lines. The distances (Å) are indicated. (C-F) Stick representation and 2Fo-Fc electron density maps contoured at 0.5 σ (2.52 rmsd) for KLHL3 Arg339 and the interfacing Cl⁻ (C and E) or a replaced water molecule (D and F) in the indicated structures. Blue meshes represent the experimental electron density. The green mesh around the water molecule represents a positive discrepancy comparing experimental data with the structure model.

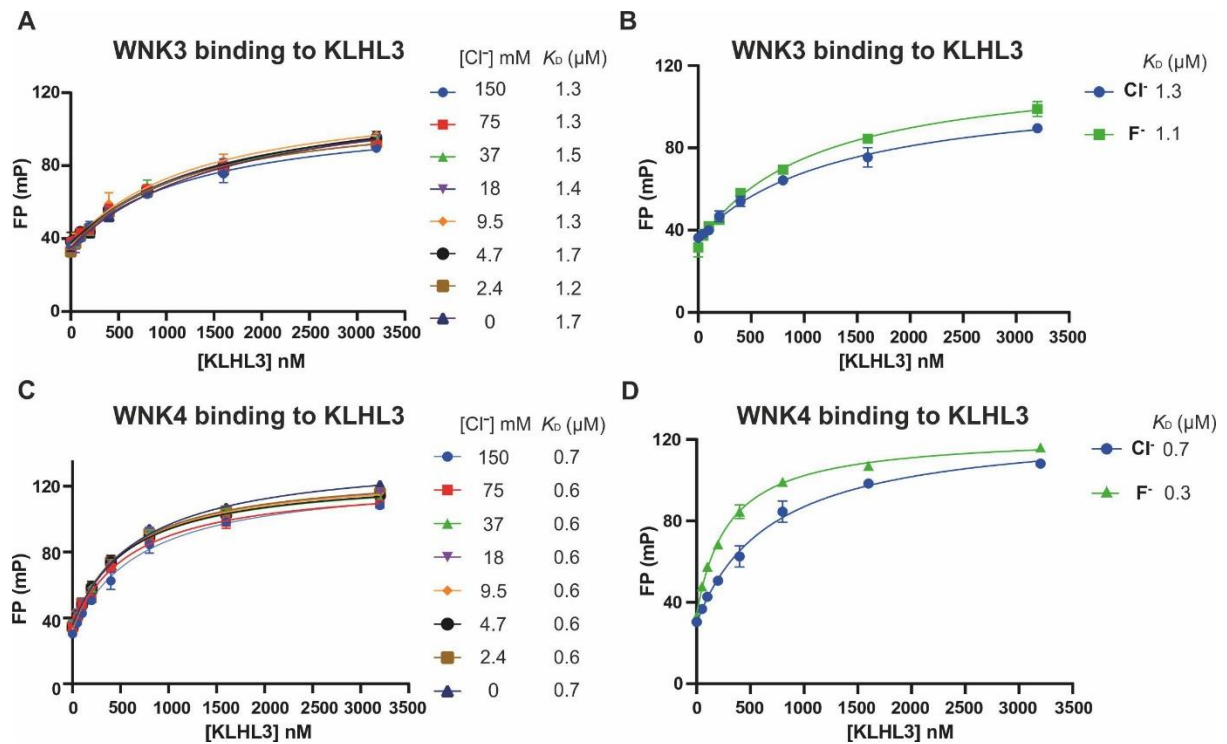


Figure S2. The effect of chloride on the interaction between KLHL3 and WNK peptides.

(A-D) Analysis of the interaction between KLHL3 and WNK peptides by fluorescence polarisation in buffers containing various Cl⁻ concentrations. Purified KLHL3 (a.a. 298-587) was diluted appropriately and mixed at a 1:1 volume ratio with 20 nM Rhodamine-110 fluorophore labelled WNK3 or WNK4 peptides to the concentration stated in the Figure, with the peptide concentration consistent at 10 nM. In panels **A** and **C**, buffers containing various Cl⁻ concentrations were balanced with phosphate buffer to keep a constant ionic strength of 154 mM. In panels **B** and **D**, 150 mM Cl⁻ or 150 mM F⁻ buffers were tested. Fluorescence polarisation measurements were recorded and corrected to the fluorescent probe alone. Each data point represents two technical replicates. For data analysis, one site-total with constant NS (slope of non-specific binding) equal to zero was assumed (model $Y = B_{max} \cdot X / (K_D + X) + \text{Background}$) and the disassociation constant was obtained. Binding curves were then generated with Prism6 using milli-polarization (mP) units.

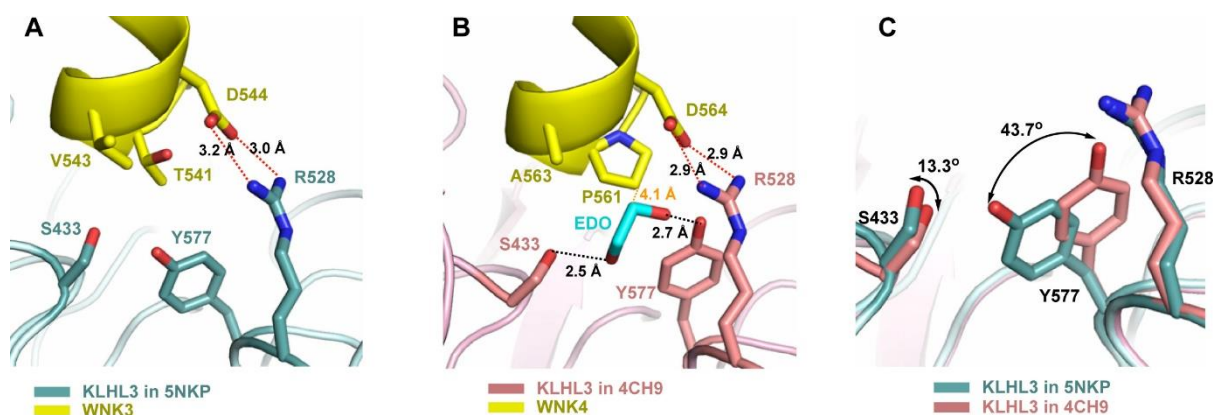


Figure S3. Side chain packing differences around the key salt bridge between WNKs and KLHL3 Arg528. (A) KLHL3 Arg528 forms a key salt bridge interaction with WNK3 Asp544. Selected side chains in the vicinity are displayed in stick representation, including KLHL3 Tyr577 as well as WNK3 Thr541 and Val543. KLHL3 is shown in green. WNK3 is shown in yellow. Salt bridge interactions are indicated with red dashed lines and labelled with distance measurements. (B) In the equivalent WNK4 complex, KLHL3 Arg528 forms a salt bridge with WNK4 Asp564. The diverged WNK4 degnon residues Pro561 and Ala563 allowed an ethylene glycol (EDO) molecule from the cryo-protectant to pack in the crystal lattice adjacent to the salt bridge and to form hydrogen bonds with the side chains of KLHL3 Ser433 and Tyr577, as indicated with black dashed lines and distance measurements. The distance between WNK4 Pro561 and the EDO is also indicated in orange. KLHL3 is shown in red, WNK4 in yellow. (C) Superposition of the two KLHL3-WNK complexes highlighting the KLHL3 residues Ser433, Arg528 and Tyr577. Side chain packing in the vicinity of KLHL3 Arg528 is altered by the WNK3-specific substitutions of Thr541 and Val543 and the shift in the position of KLHL3 Tyr577. KLHL3 in PDB 5NKP (KLHL3-WNK3 co-structure) is coloured in green and KLHL3 in PDB 4CH9 (KLHL3-WNK4 co-structure) is coloured in red.



Figure S5. Overview of WNK3 peptide hits from hypotonic treatment. Residues recovered in elastase MS/MS are shaded in grey. Modifications are labelled above residues. Peptide hits in the kinase activation segment are illustrated.

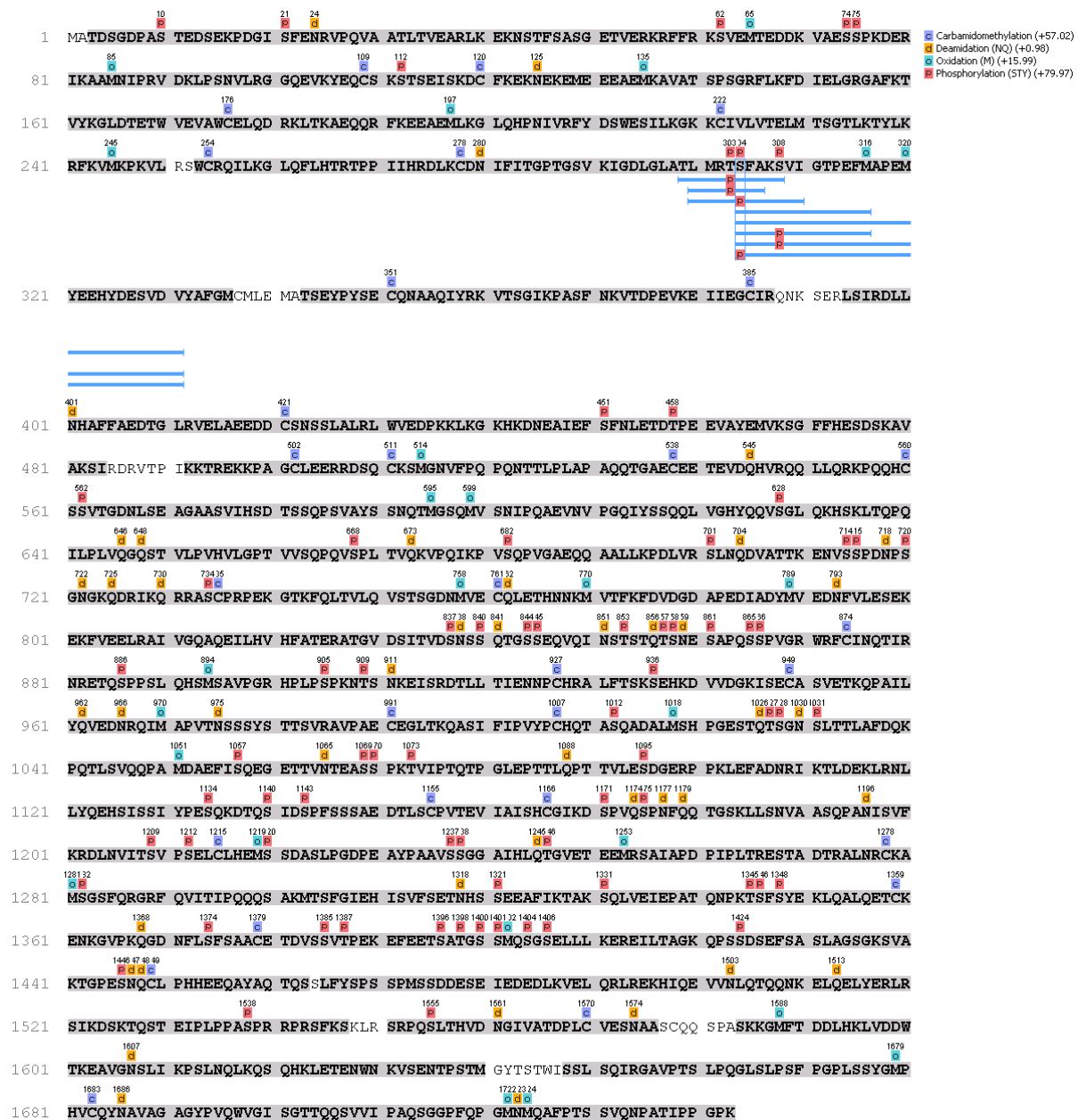


Figure S6. Overview of WNK3 peptide hits from isotonic treatment. Residues recovered in elastase MS/MS are shaded in grey. Modifications are labelled above residues. Peptide hits in the kinase activation segment are illustrated.

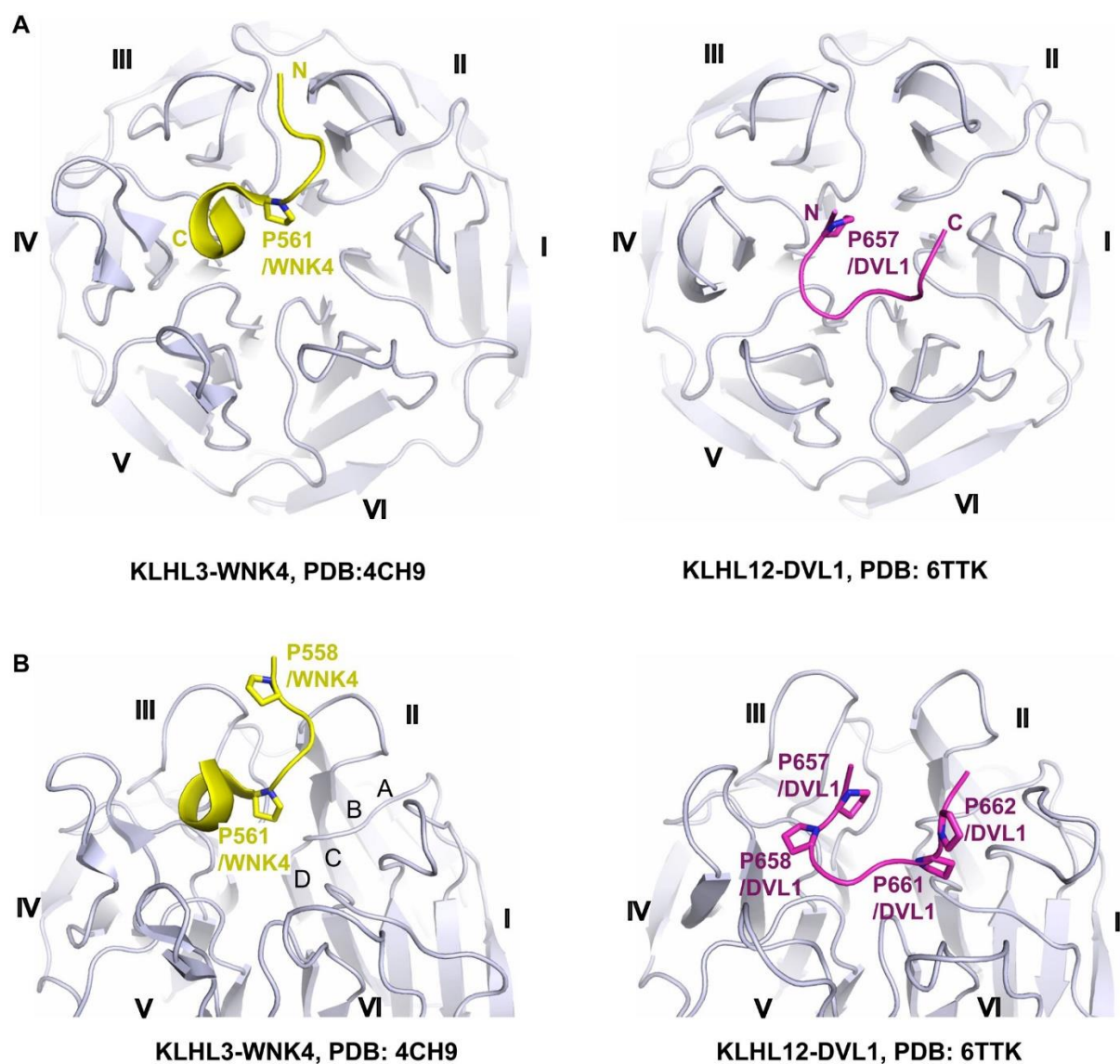


Figure S7. Diverse binding modes of Kelch-interacting PXXP motifs in substrate degrons. (A) Overviews of the KLHL3-WNK4 and KLHL12-DVL1 co-structures showing the substrate peptide conformations that contact multiple blades in the Kelch domains. WNK4 Pro561 and DVL1 Pro657 in stick representation both anchor the degron peptides in the centre of the Kelch domain binding pockets. Kelch domains are shown in grey, WNK4 in yellow and DVL1 in purple. N and C-termini of the degron peptides are labelled. Blades I to VI of the β -propeller are labelled for each Kelch domain. (B) The proline-rich motifs in the peptide degrons bind to distinct parts of the Kelch domains. Prolines in each degron motif are shown in stick representation. Blades I to VI and the β -strands A to D in Blade II are labelled for the Kelch domain.